

## Shear strength of reinforced concrete dapped-end beams

Ing-Jaung Lin<sup>†</sup>, Shyh-Jiann Hwang<sup>†</sup>, Wen-Yao Lu<sup>‡</sup> and Jiunn-Tyng Tsai<sup>‡†</sup>

*Department of Construction Engineering, National Taiwan University of Science and Technology, Taipei, Taiwan 10672, R.O.C.*

*(Received July 4, 2002, Accepted June 20, 2003)*

**Abstract.** In this study, 24 high-strength concrete dapped-end beams were tested to study the effects of the amount of main dapped-end reinforcement, the nominal shear span-to-depth ratio, and the concrete strength on the shear strength of dapped-end beams. Test results indicate that the shear strength of dapped ends increases with the increase in the amount of main dapped-end reinforcement and the concrete strength. The shear strength of dapped-end beam increases with the decrease of nominal shear span-to-depth ratio. A simplified method for determining the shear strength of reinforced concrete dapped ends is also proposed in this paper. The shear strengths predicted by the proposed method and the approach of PCI Design Handbook are compared with test results. The comparison shows that the proposed method can more accurately predict the shear strength of reinforced concrete dapped-end beams than the approach of PCI Design Handbook.

**Key words:** reinforced concrete dapped-end beams; high-strength concrete; softened strut-and-tie model.

---

### 1. Introduction

The concept of dapped-end beam is useful. It enables reduction in the construction depth of a precast concrete floor or roof structure, by recessing the supporting corbels into the depth of the supported beams (Mattock and Chan 1979). Some applications of the dapped-end are for drop-in beams between corbels (Fig. 1a), or as part of beam-to-beam connections (Fig. 1b) and for suspended spans between cantilevers (Fig. 1c).

The approach of PCI Design Handbook (1999) was developed and calibrated using test results of reinforced normal-strength concrete dapped-end beams. According to Lu *et al.* (2002) the approach of PCI Design Handbook (1999) for predicting the shear strength of dapped-end beams is less accurate than the softened strut-and-tie model (Lu *et al.* 2002). Although the softened strut-and-tie model for determining the shear strengths of beam-column joints (Hwang and Lee 1999, 2000), deep beams (Hwang *et al.* 2000a), corbels (Hwang *et al.* 2000b), squat walls (Hwang *et al.* 2001) and dapped-end beams (Lu *et al.* 2002) has been proposed, the solution procedures of the softened strut-and-tie model are tedious and further simplification is needed. A simplified method based on

---

<sup>†</sup> Professor

<sup>‡</sup> Ph.D. Candidate

<sup>‡†</sup> Former Graduate Student

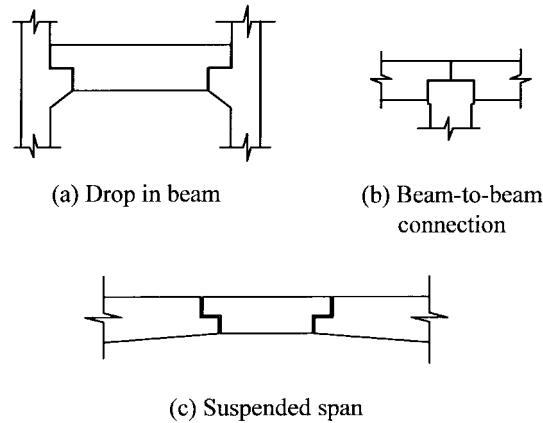


Fig. 1 Application of dapped-end beams

the softened strut-and-tie model for predicting the shear strength of discontinuity regions failing in diagonal compressions has been developed (Hwang and Lee 2002). In this paper, a test program containing twenty-four dapped-end specimens is reported. Based on the attained results and other available experimental data, the applicability of the simplified method (Hwang and Lee 2002) to dapped-end beams for predicting strength due to diagonal compression failure is examined. Considering the compressive strength of diagonal strut, the flexural capacity of nib and the tensile strength of hanger reinforcement, a simplified method to predict the shear strength of dapped-end beams is proposed. Also, the precision of the proposed model is further compared with that of the approach of PCI Design Handbook.

## 2. Experimental study

### 2.1 Experimental program

In this study, twenty-four dapped ends were tested under vertical load only. Variables considered in the tests are the amount of main dapped-end reinforcement, the nominal shear span-to-depth ratio, and the concrete strength. The dapped ends were formed on opposite ends of 3600 mm long  $200 \times 600$  mm cross section beams. All the nibs had a length of 400 mm and an overall depth of 460 mm, 380 mm and 300 mm, respectively as shown in Table 1. The dimensions of dapped ends, the sizes and amounts of reinforcement in each specimen are listed in Table 1, together with the concrete strength at the time of testing. Typical reinforcement details are shown in Fig. 2. The strain in the main dapped-end reinforcement was measured at location  $x$  in Fig. 2, and that in the hanger reinforcement at point  $y$ , using electrical resistance gages. The dapped ends were tested independently by supporting the 3600 mm long beam through the dapped end at one end of the beam, and under the beam bottom face at the opposite end. The typical arrangement for the test is shown in Fig. 3. After testing of one dapped end, damage was mostly confined to the region of that dapped end. It was therefore possible to turn the beam end-for-end, and test the other dapped end.

Table 1 Specimen details

Specimen	$f'_c$ MPa	$h$ mm	$d$ mm	$a$ mm	$a'$ mm	Main dapped-end reinforcement			Horizontal hoops		Hanger reinforcement			
						Bars	$A_s$ mm <sup>2</sup>	$f_y$ MPa	Stirrups	$A_h$ mm <sup>2</sup>	$f_{yh}$ MPa	Stirrups	$A_{vh}$ mm <sup>2</sup>	$f_{yvh}$ MPa
1	61.7	460	430	250	170	3-#6	859.6	462.2	2-#3	285.3	398.4	6-#4	1520.2	462.1
2	61.7	460	430	380	310	3-#6	859.6	462.2	2-#3	285.3	398.4	5-#4	1266.8	462.1
3	61.7	460	430	250	180	2-#6	573.0	462.2	2-#3	285.3	398.4	5-#4	1266.8	462.1
4	61.7	460	430	380	310	2-#6	573.0	462.2	2-#3	285.3	398.4	6-#3	856.0	550.1
5	61.2	460	430	250	170	3-#6	859.6	462.2	2-#3	285.3	398.4	6-#4	1520.2	462.1
6	62.6	460	430	380	310	3-#6	859.6	462.2	2-#3	285.3	398.4	5-#4	1266.8	462.1
7	57.8	460	430	250	180	2-#6	573.0	462.2	2-#3	285.3	398.4	5-#4	1266.8	462.1
8	53.3	460	430	380	310	2-#6	573.0	462.2	2-#3	285.3	398.4	6-#3	856.0	550.1
9	61.7	380	350	200	120	2-#6	573.0	462.2	2-#3	285.3	398.4	6-#4	1520.2	462.1
10	61.7	380	350	310	240	2-#6	573.0	462.2	2-#3	285.3	398.4	5-#4	1266.8	462.1
11	61.7	380	350	200	130	3-#6	859.6	462.2	2-#3	285.3	398.4	5-#4	1266.8	462.1
12	61.7	380	350	310	240	3-#6	859.6	462.2	2-#3	285.3	398.4	6-#3	856.0	550.1
13	61.8	380	350	200	120	2-#6	573.0	462.2	2-#3	285.3	398.4	6-#4	1520.2	462.1
14	60.1	380	350	310	240	2-#6	573.0	462.2	2-#3	285.3	398.4	5-#4	1266.8	462.1
15	58.3	380	350	200	130	3-#6	859.6	462.2	2-#3	285.3	398.4	5-#4	1266.8	462.1
16	63.6	380	350	310	240	3-#6	859.6	462.2	2-#3	285.3	398.4	6-#3	856.0	550.1
17	61.7	300	270	160	80	2-#6	573.0	462.2	2-#3	285.3	398.4	6-#4	1520.2	462.1
18	61.7	300	270	240	170	2-#6	573.0	462.2	2-#3	285.3	398.4	5-#4	1266.8	462.1
19	61.7	300	270	160	90	3-#6	859.6	462.2	2-#3	285.3	398.4	5-#4	1266.8	462.1
20	61.7	300	270	240	170	3-#6	859.6	462.2	2-#3	285.3	398.4	6-#3	856.0	550.1
21	71.6	300	270	160	80	2-#6	573.0	462.2	2-#3	285.3	398.4	6-#4	1520.2	462.1
22	70.5	300	270	240	170	2-#6	573.0	462.2	2-#3	285.3	398.4	5-#4	1266.8	462.1
23	69.6	300	270	160	90	3-#6	859.6	462.2	2-#3	285.3	398.4	5-#4	1266.8	462.1
24	58.9	300	270	240	170	3-#6	859.6	462.2	2-#3	285.3	398.4	6-#3	856.0	550.1

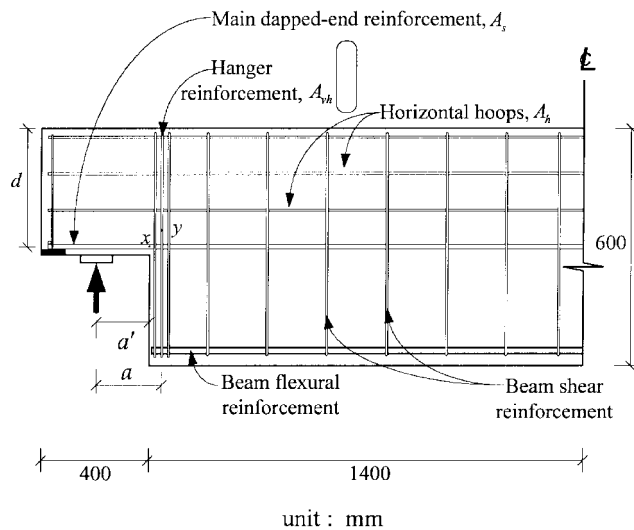


Fig. 2 Detailing of specimen

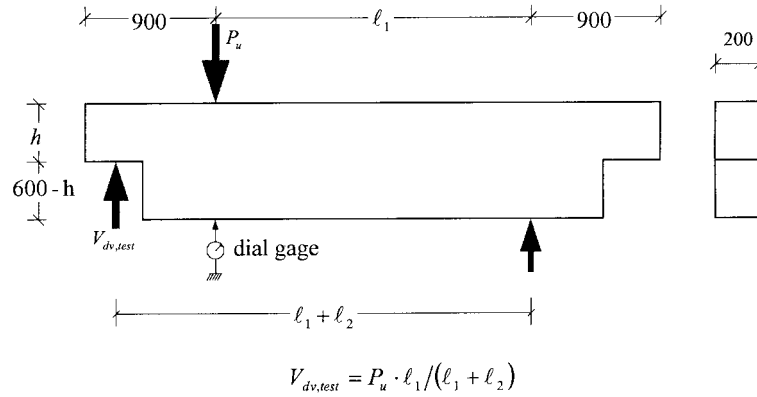


Fig. 3 Testing arrangement for dapped-end beam

## 2.2 Test results

The measured shear strength of dapped-end beams,  $V_{dv, test}$ , for each specimen obtained in the tests is summarized in Table 2. In this table, test results show that the shear strength of dapped-end

Table 2 Test results

Specimen	$a/d$	$f'_c$ MPa	$\rho f_y$ MPa	$P_u$ kN	$l_1$ mm	$l_2$ mm	$V_{dv, test}$ kN	Failure mode
1	0.58	61.7	4.62	1144	1800	670	834	Diagonal compression failure
2	0.88	61.7	4.62	778	1800	810	536	Flexural failure
3	0.58	61.7	3.08	954	1800	680	693	Diagonal compression failure
4	0.88	61.7	3.08	633	1800	810	437	Flexural failure
5	0.58	61.2	4.62	1180	1800	670	860	Diagonal compression failure
6	0.88	62.6	4.62	743	1800	810	512	Diagonal compression failure
7	0.58	57.8	3.08	867	1800	680	629	Diagonal compression failure
8	0.88	53.3	3.08	620	1800	810	427	Flexural failure
9	0.57	61.7	3.78	1056	1800	620	786	Diagonal compression failure
10	0.89	61.7	3.78	657	1800	740	466	Flexural failure
11	0.57	61.7	5.68	1107	1800	630	820	Diagonal compression failure
12	0.89	61.7	5.68	759	1800	740	538	Tensile failure
13	0.57	61.8	3.78	984	1800	620	732	Diagonal compression failure
14	0.89	60.1	3.78	524	1800	740	371	Diagonal compression failure
15	0.57	58.3	5.68	1032	1800	630	764	Diagonal compression failure
16	0.89	63.6	5.68	754	1800	740	534	Tensile failure
17	0.59	61.7	4.90	932	1800	580	705	Diagonal compression failure
18	0.89	61.7	4.90	646	1800	670	471	Diagonal compression failure
19	0.59	61.7	7.36	988	1800	590	744	Diagonal compression failure
20	0.89	61.7	7.36	687	1800	670	501	Diagonal compression failure
21	0.59	71.6	4.90	900	1800	580	681	Diagonal compression failure
22	0.89	70.5	4.90	696	1800	670	507	Diagonal compression failure
23	0.59	69.6	7.36	1025	1800	590	772	Diagonal compression failure
24	0.89	58.9	7.36	747	1800	670	544	Diagonal compression failure

beams increases with the decrease of nominal shear span-to-depth ratio ( $a/d$ ). As shown in Table 2, the shear strength of dapped-end beams increases with the increase of the parameter of main dapped-end reinforcement ( $\rho f_y$ ). For the same  $\rho f_y$  and nominal shear span-to-depth ratio, the shear strength of dapped-end beams increases with the increase of the concrete strength (Table 2).

The observed load-displacement relationships for the 24 specimens are shown in Fig. 4. The typical cracking pattern for dapped-end beams tested is shown in Fig. 5. The shear action in the nib of a dapped-end beam leads to compression in a diagonal direction and tension perpendicular thereto, several diagonal cracks form due to the diagonal tension. Similar to the deep beams and corbels, dapped-end beams do not fail immediately due to the formation of the diagonal cracks. The concrete between the diagonal cracks constitutes the diagonal compression strut, the external shear

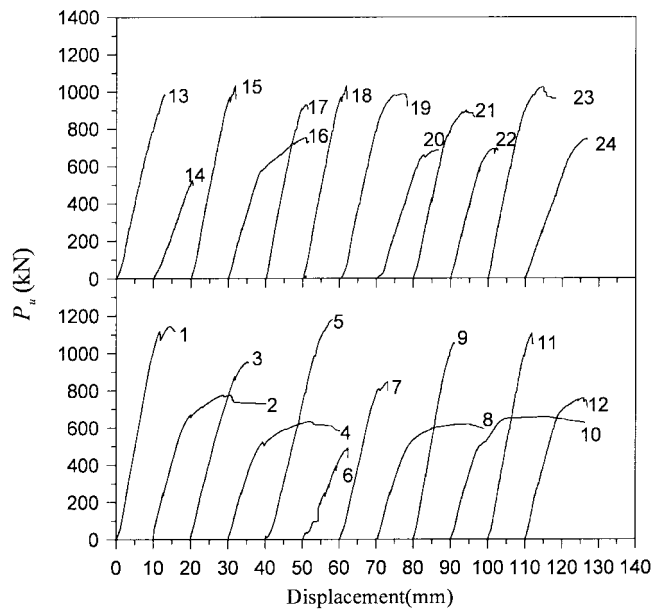


Fig. 4 Load versus displacement

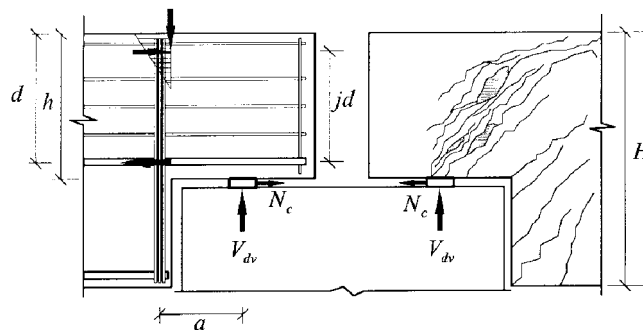


Fig. 5 Typical failure in dapped ends tested

transferred by the diagonal compression strut, and the failure mode could be the diagonal compression failure, the flexural failure and the tensile failure (failure initiated by the yielding of hanger bars) as shown in Table 2.

### 3. Softened strut-and-tie model

Fig. 6 shows the loads acting on a dapped-end beam and the proposed force transferring mechanisms in view of the strut-and-tie model. The outward horizontal force  $N_c$  is balanced by the tension in the primary steel ( $T$ ) and the effect of shifting of  $N_c$  is neglected in this study for simplicity. By taking into account the distances between couples (Fig. 6), it will be sufficiently accurate to express the following relationship between vertical and horizontal shears.

$$\frac{V_{dv}}{V_{dh}} \approx \frac{jd}{a'} \tag{1}$$

where,  $V_{dv}$  and  $V_{dh}$  are the vertical and horizontal shear forces, respectively;  $jd$  is the distance of the lever arm from the resultant compressive force to the centroid of the flexural tension reinforcement. According to Appendix A of ACI Code (2002), the discontinuity is defined as an abrupt change in geometry or loading, the actual shear span  $a'$  is measured from the center of support to the interface between the nib and the full-depth beam. The horizontal shear force  $V_{dh}$  is equal to the resultant

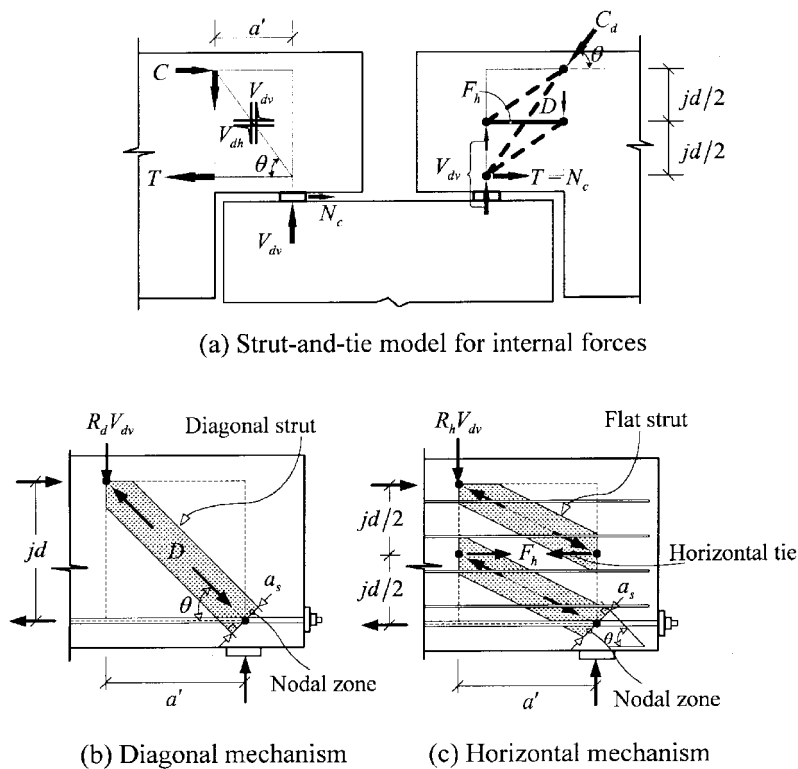


Fig. 6 Strut-and-tie model for dapped ends

compressive force  $C$  at section due to flexure, i.e.  $V_{dh} = C = T - N_c$  (Fig. 6). According to linear bending theory, the lever arm  $jd$  of a singly reinforced rectangular section can be estimated as

$$jd = d - kd/3 \quad (2)$$

where,  $d$  is the effective depth of the nib;  $kd$  is the depth of compression zone at the section; and coefficient  $k$  can be defined as,

$$k = \sqrt{(n\rho_f)^2 + 2n\rho_f} - n\rho_f \quad (3)$$

where,  $n$  is the modular ratio of elasticity;  $\rho_f = A_f/bd$ ,  $\rho_f$  is the ratio of primary tensile steel resisting moment;  $A_f = A_s - A_n$ ,  $A_f$  is the area of primary tensile steel resisting moment;  $A_s$  is the area of main dapped-end reinforcement;  $A_n$  is the area of primary tensile steel resisting tensile force ( $N_c$ ) and  $b$  is the width of the nib.

### 3.1 Macromodel

Fig. 6 shows the proposed softened strut-and-tie model, which is composed of the diagonal and horizontal mechanisms. The diagonal mechanism (Fig. 6) is a diagonal compression strut whose angle of inclination,  $\theta$ , is defined as,

$$\theta = \tan^{-1}\left(\frac{jd}{a'}\right) \quad (4)$$

The direction of the principal compressive stress of the concrete is also assumed to coincide with the direction of the diagonal concrete strut.

The effective area of the diagonal compression strut  $A_{str}$  is defined as

$$A_{str} = a_s \times b_s \quad (5)$$

where,  $a_s$  is the depth of the diagonal strut; and  $b_s$  is the width of the diagonal strut which can be taken as the width of the nib.

The depth of the diagonal strut ( $a_s$ ) depends on its end condition provided by the compression zone at the interface between the nib and full depth beam. It is intuitively assumed that

$$a_s = kd \quad (6)$$

The horizontal mechanism (Fig. 6) includes one horizontal tie and two flat struts. The horizontal tie is made up of the horizontal hoops. When computing the cross area of the horizontal tie, it is roughly assumed that the horizontal hoops within the center half of the dapped end is fully effective, and the other horizontal hoops is included as 50% effective (Hwang and Lee 1999, 2000).

### 3.2 Equilibrium conditions

The diagonal compression ( $C_d$ ) of a dapped-end beam can be estimated as (Fig. 6)

$$C_d = -D + \frac{F_h}{\cos \theta} = \frac{V_{dv}}{\sin \theta} \quad (7)$$

where,  $D$  is the compression force in the diagonal strut; and  $F_h$  is the tension force in the horizontal tie. The ratios of the diagonal compression assigned between the two mechanisms are assumed as

$$-D : \frac{F_h}{\cos \theta} = R_d : R_h \quad (8)$$

where,  $R_d$  and  $R_h$  are the ratios of the diagonal compression carried by the diagonal and horizontal mechanisms, respectively. The values of  $R_d$ , and  $R_h$  are defined as

$$R_d = 1 - \gamma_h \quad (9)$$

$$R_h = \gamma_h \quad (10)$$

where,  $\gamma_h$  is the fraction of diagonal compression transferred by the horizontal tie in the absence of the vertical tie. Based on the study of the principal stress pattern from a linear-elastic finite element analysis (Schäfer 1996),  $\gamma_h$  can be defined as

$$\gamma_h = \frac{2 \tan \theta - 1}{3}, \quad \text{but } 0 \leq \gamma_h \leq 1 \quad (11)$$

Eq. (11) indicates that there are two borderline cases, namely, that the entire diagonal compression is carried by the horizontal mechanism for  $\theta \geq \tan^{-1}(2)$  and that the entire diagonal compression is transferred by the diagonal mechanism for  $\theta \leq \tan^{-1}(1/2)$ .

Previous studies (Hwang and Lee 1999, 2000) have shown that three load paths exist in transferring diagonal compression for the cases of  $\tan^{-1}(1/2) < \theta < \tan^{-1}(2)$ . For dapped ends without vertical stirrups in the above cases, the concrete tension ties in the vertical direction will develop first, but will eventually crack. Those dapped ends transmit the diagonal compression effectively with the diagonal and horizontal mechanisms, but the cracks perpendicular to the vertical direction are not restrained.

The maximum compressive stress  $-\sigma_{d, \max}$ , resulting from the summation of the compressive forces from the diagonal and flat struts (Fig. 6), on the nodal zone, can be estimated as

$$-\sigma_{d, \max} = \frac{1}{A_{str}} \left\{ -D + \frac{F_h}{\cos \theta} \left( 1 - \frac{\sin^2 \theta}{2} \right) \right\} \quad (12)$$

If the bearing pressure on the nodal zone  $\sigma_{d, \max}$  reaches the capacity of the concrete, the diagonal compressive strength of the dapped-end beam is attained.

### 3.3 Constitutive laws

The cracked reinforced concrete in compression has been observed to exhibit lower strength than uniaxially compressed concrete (Vecchio and Collins 1993, Zhang and Hsu 1998). This phenomenon of strength reduction is called the softening of concrete. It is believed that the diagonal compressive strength of dapped-end beams should also be governed by the softening effect of concrete (Lu *et al.* 2002). According to Zhang and Hsu (1998), the softened stress-strain curve of the cracked concrete (Fig. 7) is represented as follows:

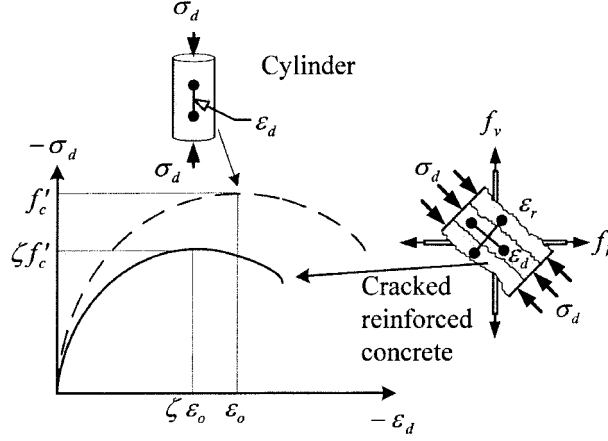


Fig. 7 Softening of compressive stress-strain curve due to transverse tensile strains

$$\sigma_d = -\zeta f'_c \left[ 2 \left( \frac{-\epsilon_d}{\zeta \epsilon_o} \right) - \left( \frac{-\epsilon_d}{\zeta \epsilon_o} \right)^2 \right] \quad \text{for} \quad \frac{-\epsilon_d}{\zeta \epsilon_o} \leq 1 \quad (13)$$

$$\sigma_d = -\zeta f'_c \left[ 1 - \left( \frac{-\epsilon_d / \zeta \epsilon_o - 1}{2 / \zeta - 1} \right)^2 \right] \quad \text{for} \quad \frac{-\epsilon_d}{\zeta \epsilon_o} > 1 \quad (14)$$

$$\zeta = \frac{5.8}{\sqrt{f'_c}} \frac{1}{\sqrt{1 + 400 \epsilon_r}} \leq \frac{0.9}{\sqrt{1 + 400 \epsilon_r}} \quad (15)$$

where,  $\sigma_d$  is the average principal stress of concrete in the  $d$ - direction;  $\zeta$  is the softening coefficient;  $f'_c$  is the compressive strength of a standard concrete cylinder in units of MPa;  $\epsilon_d$  and  $\epsilon_r$  are the average principal strains in the  $d$ - and  $r$ - directions, respectively; and  $\epsilon_o$  is the concrete cylinder strain corresponding to the cylinder strength  $f'_c$ . The value of  $\epsilon_o$  can be defined approximately as (Foster and Gilbert 1996)

$$\epsilon_o = 0.002 + 0.001 \left( \frac{f'_c - 20}{80} \right) \quad \text{for} \quad 20 \leq f'_c \leq 100 \text{MPa} \quad (16)$$

If the stress-strain relationship of mild steel for the horizontal shear reinforcement is assumed to be elastic-perfectly plastic, then

$$f_h = E_s \epsilon_h \quad \text{for} \quad \epsilon_h < \epsilon_{yh} \quad (17a)$$

$$f_h = f_{yh} \quad \text{for} \quad \epsilon_h \geq \epsilon_{yh} \quad (17b)$$

where,  $E_s$  is the elastic modulus of the steel;  $f_h$  and  $\epsilon_h$  are the average tensile stress and strain of the horizontal tie, respectively; and  $f_{yh}$  and  $\epsilon_{yh}$  are the yield stress and strain of the horizontal hoops, respectively. Based on the simplified constitutive equations for steel, the relationships between force and strain of the horizontal tie can be constructed as

$$F_h = A_{th} E_s \epsilon_h \leq F_{yh} \quad (18)$$

where  $A_{th}$  is the area of the horizontal ties;  $F_{yh}$  is the yielding force of the horizontal ties.

### 3.4 Compatibility condition

A rigorous analysis dealing with two-dimensional membrane elements should satisfy Mohr's circular compatibility condition. The compatibility equation employed in this paper is the first strain invariant.

$$\varepsilon_r + \varepsilon_d = \varepsilon_h + \varepsilon_v \quad (19)$$

where,  $\varepsilon_h$  and  $\varepsilon_v$  are the average normal strains in the  $h$ - and  $v$ - directions, respectively.

Details of the solution procedure of softened strut-and-tie model are presented elsewhere (Hwang *et al.* 2000b).

## 4. The proposed method

A case study on shear strength prediction of corbels (Hwang *et al.* 2000b) had shown that a bilinear relationship exists between the shear strength and the horizontal reinforcement. The concrete strength appears to set an upper limit value of horizontal tie, below which (under-reinforced) the horizontal hoops reach yielding before failure, at which (balanced point) the horizontal hoops reach yielding at failure, and above which (over-reinforced) the horizontal hoops do not yield (Hwang *et al.* 2000b). For the under-reinforced corbels, the shear capacities are increased with increasing horizontal hoops at a greater rate (Hwang *et al.* 2000b), because the horizontal hoops are effective in augmenting the force of tension tie  $F_h$ . For the over-reinforced corbels, the shear capacities are increased with increasing horizontal hoops at a much lower rate (Hwang *et al.* 2000b), because the additional horizontal hoops beyond the balanced amount is only effective in retarding the softening effect of concrete.

The foregoing observations reveal that the beneficial effect of the additional tension tie beyond the balanced amount on diagonal compressive strength could be neglected. Moreover, the linear relationship between the diagonal compressive strength and the amount of tension tie indicates that the technique of linear interpolation can be used for the under-reinforced dapped-end beams for diagonal compressive strength prediction.

If a dapped-end contains the horizontal hoops, additional load paths will carry the diagonal compression. This will activate more concrete for diagonal compressive resistance, and thus enhances the diagonal compressive strength. A factor representing the beneficial effect of the tie force on the diagonal compressive strength can take the form (Hwang and Lee 2002)

$$K = \frac{C_d}{-\sigma_{d, \max} \times A_{str}} = \frac{-D + \frac{F_h}{\cos \theta}}{-D + \frac{F_h}{\cos \theta} \left(1 - \frac{\sin^2 \theta}{2}\right)} \geq 1 \quad (20)$$

where,  $K$  is defined as the strut-and-tie index.

The nominal diagonal compressive strength  $C_{d,n}$  is estimated as

$$C_{d,n} = K \zeta f'_c A_{str} \quad (21)$$

4.1 Approximation of softening effect

The extent of softening of the concrete is directly related to the value of the principal tensile strain  $\epsilon_r$  (Vecchio and Collins 1993, Zhang and Hsu 1998). It was recommended that the value of  $\epsilon_r$  be limited to the strain level at which the yielding of the reinforcement crossing the crack occur (Vecchio and Collins 1993). In this study, the values of  $\epsilon_h$  and  $\epsilon_v$  are limited by 0.002 (Hwang *et al.* 2000b). From past experience (Hwang and Lee 1999, 2000), the variable  $\epsilon_d$  can be relegated to a constant of  $-0.001$  for strength estimation. Therefore, the value of  $\epsilon_r$  is taken as 0.005 ( $0.002 + 0.002 + 0.001$ ) as per Eq. (19). As a result, the softening coefficient  $\zeta$  can be approximated by Eq. (15) as

$$\zeta \approx \frac{3.35}{\sqrt{f'_c}} \leq 0.52 \tag{22}$$

4.2 Strut-and-tie index

There are two possible resisting mechanisms for dapped-end subjected to diagonal compressions. They are the diagonal mechanism (Fig. 8) and the diagonal plus horizontal mechanisms (Fig. 9). If a dapped-end is not detailed with any horizontal hoop, only the diagonal strut carries the diagonal compression, as shown in Fig. 8. Recalling Eq. (20), we can define the diagonal strut index  $K_d$  as

$$K_d = \frac{-D}{-D} = 1 \tag{23}$$

For the case of the over-reinforced dapped-end, the concrete strut would reach its strength while the horizontal tie remains in the elastic range. The additional contribution of the sufficient horizontal tie for the diagonal compressive strength can be estimated by Eq. (24) as [Fig. 9(b), Hwang and Lee 2002].

$$\bar{K}_h = \frac{(1 - \gamma_h) + \gamma_h}{(1 - \gamma_h) + \gamma_h \left(1 - \frac{\sin^2 \theta}{2}\right)} \geq 1 \tag{24}$$

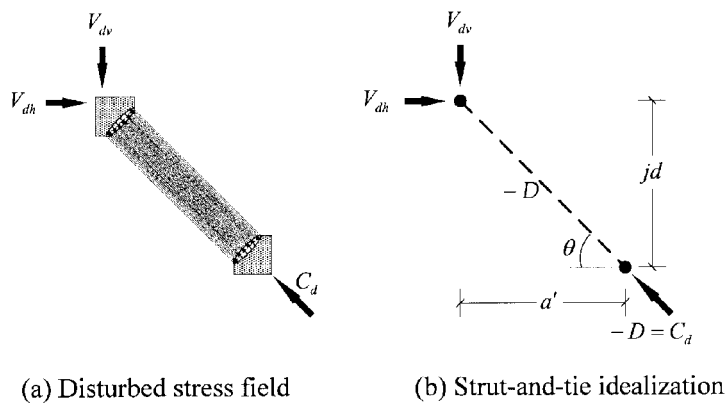


Fig. 8 Diagonal mechanism

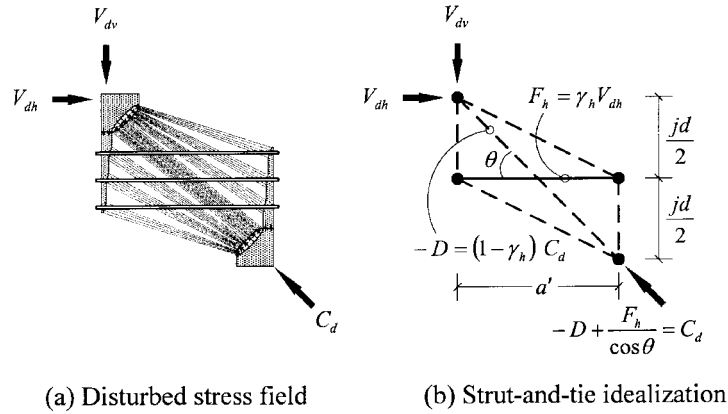


Fig. 9 Diagonal and horizontal mechanisms

where,  $\bar{K}_h$  is the horizontal tie index with sufficient horizontal reinforcement. Eq. (24) can be further simplified as (Hwang and Lee 2002)

$$\bar{K}_h \approx \frac{1}{1 - 0.2(\gamma_h + \gamma_h^2)} \tag{25}$$

The balanced amount of the horizontal tie force  $\bar{F}_h$ , at which the horizontal tie reaches yielding at failure for the case shown in Fig. 9(b), can be defined as (Hwang and Lee 2002)

$$\bar{F}_h = \gamma_h \times (\bar{K}_h \zeta_c' A_{str}) \times \cos \theta \tag{26}$$

For the under-reinforced cases, the horizontal tie index  $K_h$  can be approximated by linear interpolation using the balanced amount of the horizontal tie force (Hwang and Lee 2002).

$$K_h = 1 + (\bar{K}_h - 1) \frac{F_{yh}}{\bar{F}_h} \leq \bar{K}_h \tag{27}$$

In the absence of the vertical hoops of dapped ends studied, it is recommended that the strut-and-tie index can be estimated as (Hwang and Lee 2002)

$$K = K_d + K_h - 1 = K_h \tag{28}$$

The shear strength of dapped ends based on the diagonal crushing failure can be calculated as

$$V_{dv, calc} = C_{d,n} \times \sin \theta \tag{29}$$

### 4.3 Shear strength due to flexural failure

There are three major failure modes for reinforced concrete dapped-end beams such as diagonal compression failure, flexural failure and tensile failure, respectively. The strength of dapped-end beams is taken as the smallest value of the above three failure modes. The shear force based on the flexural strength of the nib (Fig. 2) can be estimated as follows:

$$V_{dv, calc} = \frac{M_n - N_c(h - d)}{a'} \quad (30a)$$

$$M_n = A_f f_y \left( d - \frac{A_f f_y}{1.7 f'_c b} \right) \quad (30b)$$

where,  $M_n$  is the nominal flexural strength of the nib and  $h$  is the overall depth of the nib.

#### 4.4 Shear strength due to tensile failure

The shear force based on the tensile strength (Fig. 2) can be estimated as follow:

$$V_{dv, calc} = A_{vh} f_{yv} \quad (31)$$

where  $A_{vh}$  and  $f_{yv}$  are the area and yield strength of the hanger bars, respectively.

### 5. Approach of PCI Design Handbook

According to the PCI Design Handbook (1999), the predicted shear strength of dapped-end beams can be limited by the tensile strength of the hanger bars as stated in Eq. (31).

The shear force can be determined by the flexural strength of the nib.

$$V_{dv, calc} = \frac{M_n - N_c(h - d)}{a} \quad (32)$$

It is noted that Eq. (32) uses the nominal shear span ( $a$ ) instead of the actual shear span ( $a'$ ).

According to the PCI Design Handbook (1999), the shear strength can be estimated by the shear-friction concept.

$$V_{dv, calc} = \sqrt{6.895 \mu \lambda b h (A_s f_y + A_h f_{yh} - N_c)} \quad (33a)$$

where, friction coefficient  $\mu = 1.4 \lambda$ ;  $\lambda$  is coefficient for type of concrete, for normal weight concrete,  $\lambda = 1.0$ ;  $A_h$  is the area of the horizontal hoops. According to the PCI Design Handbook (1999), the shear strength of the dapped-end beams is limited as

$$V_{dv, calc} \leq 0.3 \lambda^2 f'_c b h \quad (33b)$$

$$V_{dv, calc} \leq 6.895 \lambda^2 b h \quad (33c)$$

According to the PCI Design Handbook (1999), the shear strength should also be determined by the beam type shear strength of the nib.

$$V_{dv, calc} = A_v f_{yv} + A_h f_{yh} + 0.166 \sqrt{f'_c} \lambda b d \quad (34)$$

where,  $A_v$  is the area of the vertical hoops of the nib.

## 6. Experimental verification

A total of 44 test specimens and their results were used to verify the analytical models. These are the test results of this study, and Mattock and Chan (1979) and Lu *et al.* (2002). Table 3 compares the measured failure loads with the predictions of the proposed method and the approach of PCI Design Handbook. Accuracy for the analytical model is gauged in terms of a strength ratio, which is defined as the ratio of the measured strength to the calculated strength.

In this study, the mean of the measured-to-calculated strength ratio is 1.22 with a coefficient of variation of 0.11 for the proposed method (Table 3). More conservative but scattered predictions are obtained from the approach of PCI Design Handbook. The mean of the measured-to-calculated strength ratio is 2.83 with a coefficient of variation of 0.27 (Table 3).

Fig. 10 shows the effect of the nominal shear span-to-depth ratio  $a/d$  on the shear strength predictions for dapped-end beams. The proposed method consistently predicts the shear strength of

Table 3 Experimental verification

Specimen	$a/d$	$f'_c$ MPa	$f_{yh}$ MPa	$\rho f_y$ MPa	$N_c$ kN	Proposed method				PCI Approach <sup>1999</sup>						
						$V_{dv, calc}(kN)$			$V_{dv, test}$	$V_{dv, calc}(kN)$				$V_{dv, test}$		
						Strut- and-tie	Eq. (30)	Eq. (31)	$V_{dv, calc}$	Eq. (31)	Eq. (32)	Eq. (33)	Eq. (34)	$V_{dv, calc}$		
This study																
1	0.58	61.7	398	4.62	0	666	961	702	1.25	702	653	634	226	3.69		
2	0.88	61.7	398	4.62	0	531	527	585	1.02	585	430	634	226	2.37		
3	0.58	61.7	398	3.08	0	567	614	585	1.22	585	442	580	226	3.07		
4	0.88	61.7	398	3.08	0	456	357	471	1.22	471	291	580	226	1.93		
5	0.58	61.2	398	4.62	0	665	960	702	1.29	702	653	634	225	3.82		
6	0.88	62.6	398	4.62	0	533	527	585	0.97	585	430	634	227	2.26		
7	0.58	57.8	398	3.08	0	558	623	585	1.13	585	441	580	222	2.83		
8	0.88	53.3	398	3.08	0	438	355	471	1.20	471	290	580	218	1.96		
9	0.57	61.7	398	3.78	0	543	745	702	1.45	702	447	524	205	3.83		
10	0.89	61.7	398	3.78	0	418	372	585	1.25	585	288	524	205	2.27		
11	0.57	61.7	398	5.68	0	609	1012	585	1.40	585	658	524	205	4.00		
12	0.89	61.7	398	5.68	0	484	548	471	1.14	471	424	524	205	2.62		
13	0.57	61.8	398	3.78	0	544	745	702	1.35	702	447	524	205	3.57		
14	0.89	60.1	398	3.78	0	415	372	585	1.00	585	288	524	204	1.82		
15	0.57	58.3	398	5.68	0	600	1008	585	1.31	585	655	524	202	3.69		
16	0.89	63.6	398	5.68	0	488	549	471	1.13	471	425	524	206	2.59		
17	0.59	61.7	398	4.90	0	502	852	702	1.40	702	426	414	184	3.83		
18	0.89	61.7	398	4.90	0	378	401	585	1.25	585	284	414	184	2.56		
19	0.59	61.7	398	7.36	0	550	1108	585	1.35	585	623	414	184	4.04		
20	0.89	61.7	398	7.36	0	434	587	471	1.15	471	416	414	184	2.72		
21	0.59	71.6	398	4.90	0	520	858	702	1.31	702	429	414	190	3.59		
22	0.89	70.5	398	4.90	0	392	403	585	1.29	585	286	414	190	2.69		
23	0.59	69.6	398	7.36	0	567	1118	585	1.36	585	629	414	188	4.10		
24	0.89	58.9	398	7.36	0	429	585	471	1.27	471	414	414	182	2.98		
									AVG	1.24					AVG	3.03
									COV	0.10					COV	0.25

Table 3 Continued

Specimen	<i>a/d</i>	$f'_c$ MPa	$f_{yh}$ MPa	$\rho f_y$ MPa	$N_c$ kN	Proposed method				PCI Approach <sup>1999</sup>					
						$V_{dv, calc}$ (kN)			$V_{dv, test}$	$V_{dv, calc}$ (kN)				$V_{dv, test}$	
						Strut-and-tie	Eq. (30)	Eq. (31)	$V_{dv, calc}$	Eq. (31)	Eq. (32)	Eq. (33)	Eq. (34)	$V_{dv, calc}$	
Mattock and Chan <sup>1979</sup>															
1A	0.59	33.6	462	1.89	0	141	161	192	1.02	192	111	191	64	2.24	
1B	0.59	30.5	455	6.54	133	178	206	199	1.07	199	143	244	91	2.09	
2A	0.59	33.0	462	2.85	0	182	238	131	1.36	131	165	246	94	1.90	
2B	0.59	30.9	461	6.54	111	191	259	134	1.27	134	179	261	92	1.83	
3A	0.59	37.0	448	2.83	0	194	238	162	1.33	162	165	244	94	2.30	
3B	0.59	31.6	484	6.95	125	192	260	170	1.04	170	180	264	95	1.85	
4A	0.59	31.6	436	2.83	0	175	236	163	1.16	163	164	243	90	2.11	
4B	0.59	29.4	462	6.95	125	183	259	169	1.05	169	179	262	92	1.93	
									AVG	1.16				AVG	2.03
									COV	0.12				COV	0.09
Lu <i>et al.</i> <sup>2002</sup>															
1	0.56	34.0	368	7.39	0	514	1170	545	1.09	545	624	414	157	3.57	
2	0.59	62.6	368	7.39	0	652	1247	654	1.08	654	624	414	176	4.01	
3	0.59	69.2	368	7.39	0	670	1256	654	1.23	654	628	414	180	3.96	
4	0.89	34.0	368	7.39	0	345	585	356	1.04	356	390	414	157	2.29	
5	0.83	62.6	368	7.39	0	449	624	436	1.18	436	443	414	176	2.91	
6	0.81	69.2	368	7.39	0	462	628	436	1.19	436	457	414	180	2.89	
7	0.52	33.7	368	5.08	0	460	817	436	1.15	436	467	414	157	2.92	
8	0.54	62.6	368	5.08	0	578	852	436	1.37	436	470	414	176	3.40	
9	0.54	69.2	368	5.08	0	594	856	436	1.47	436	472	414	180	3.57	
10	0.83	33.7	368	5.08	0	306	408	297	0.98	297	290	414	157	1.85	
11	0.85	62.6	368	5.08	0	395	426	297	1.18	297	296	414	176	1.99	
12	0.85	69.2	368	5.08	0	407	428	297	1.32	297	298	414	180	2.18	
									AVG	1.19				AVG	2.96
									COV	0.12				COV	0.25
<b>Total</b>	<b>44</b>							<b>AVG</b>	<b>1.22</b>				<b>AVG</b>	<b>2.83</b>	
									<b>COV</b>	<b>0.11</b>				<b>COV</b>	<b>0.27</b>

the dapped-end beams with *a/d* ratios between 0.52 and 0.89 (Fig. 10b and Table 3). But a greater scattering is found for the PCI predictions, with more conservative estimations for low *a/d* ratio (Fig. 10c). Test results show that the shear strength of dapped-end beams increases with decreasing *a/d* (Fig. 10a). In the softened strut-and-tie model,  $\theta$  increases with decreasing *a/d*, the higher capacity will be predicted for a larger  $\theta$  (smaller *a/d* value) as stated in Eq. (29). As beam type shear concept is adopted in shear strength calculation (Eq. 34), the PCI predictions cannot adequately simulate the highly influential factor of the *a/d* ratio.

Fig. 11 shows the effect of the concrete strength on the shear strength predictions for dapped-end beams. Fig. 11(a) reveals that the shear strength of dapped-end beams increases with the increase of the concrete strength. On the whole, the precision of the proposed method is very consistent for a broad range of concrete strength (Fig. 11b). But a greater scattering is found for the PCI

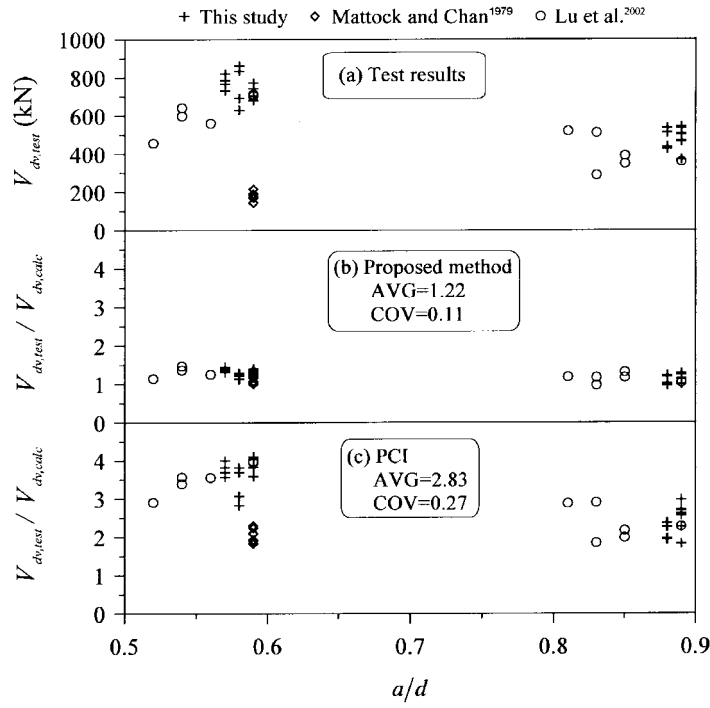


Fig. 10 Effect of nominal shear span-to-depth ratio on shear strength prediction

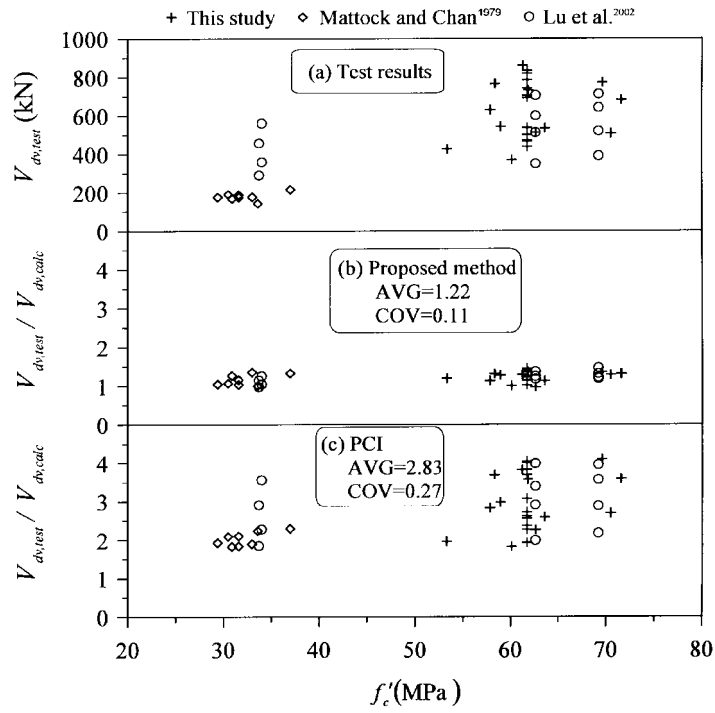


Fig. 11 Effect of concrete strength on shear strength prediction

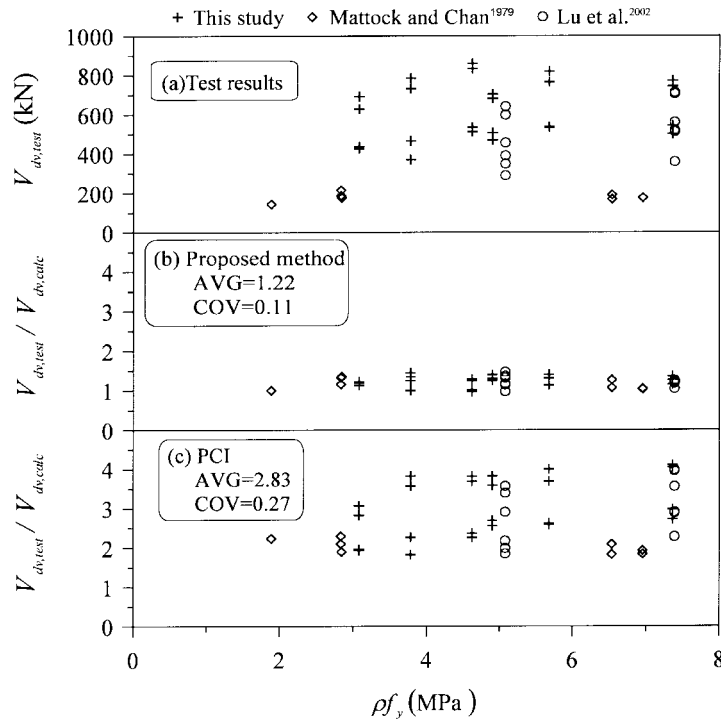


Fig. 12 Effect of main dapped-end reinforcement on shear strength prediction

predictions, with more conservative estimations for the high-strength concrete dapped-end beams (Fig. 11c). The beam type shear concept adopted in PCI predictions considers the shear strength of the nib as partly derived from the tensile strength of concrete (Eq. 34), but this does not correlate well with the observed failure phenomenon of concrete crushing in the diagonal strut. Based on the observation of concrete crushing in the diagonal direction, the softened strut-and-tie model recognizes that the diagonal compressive strength of dapped-end beams depends on the softened compressive strength of concrete.

Fig. 12 shows the effect of the main dapped-end reinforcement on the shear strength predictions for dapped-end beams. The proposed method consistently predicts the shear strength of dapped-end beams for a broad range of  $\rho f_y$  (Fig. 12b). Apparently, the PCI approach cannot adequately simulate the effect of  $\rho f_y$  in dapped-end beams (Fig. 12c).

### 7. Conclusions

In this study, 24 high-strength concrete dapped-end beams were tested. A simplified method for determining the shear strength of dapped-end beams has been made. Based on available test results in the literature and their comparison with predictions of the proposed method and the approach of PCI Design Handbook, the following conclusions can be made:

1. The shear strength of dapped ends increases with the increase of the amount of main dapped-end reinforcement and the concrete strength (Table 2). The shear strength of dapped-end beams

- increases with the decrease of the nominal shear span-to-depth ratio (Table 2).
2. The major failure modes of dapped-end beams can be categorized as diagonal compression failure, flexural failure and tensile failure (Table 2).
  3. The performance of the proposed method is better than that of the PCI approach for all parameters under comparison (Figs. 10-12). It is therefore recommended that the current shear design procedure for dapped-end beams be reformed to incorporate in the proposed method.

## Reference

- American Concrete Institute (2002), "Building code requirements for structural concrete", ACI 318-02 and Commentary (ACI 318R-02), Farmington Hills, Mich.
- Foster, S.J. and Gilbert, R.I. (1996), "The design of nonflexural members with normal and high-strength concrete", *ACI Struct. J.*, **93**(1), 3-10.
- Hwang, S.J. and Lee, H.J. (1999), "Analytical model for predicting shear strengths of exterior reinforced concrete beam-column joints for seismic resistance", *ACI Struct. J.*, **96**(5), 846-857.
- Hwang, S.J. and Lee, H.J. (2000), "Analytical model for predicting shear strengths of interior reinforced concrete beam-column joints for seismic resistance", *ACI Struct. J.*, **97**(1), 34-44.
- Hwang, S.J., Lu, W.Y. and Lee, H.J. (2000a), "Shear strength prediction for deep beams", *ACI Struct. J.*, **97**(3), 367-376.
- Hwang, S.J., Lu, W.Y. and Lee, H.J. (2000b), "Shear strength prediction for reinforced concrete corbels", *ACI Struct. J.*, **97**(4), 543-552.
- Hwang, S.J., Fang, W.H., Lee, H.J. and Yu, H.W. (2001), "Analytical model for predicting shear strength of squat walls", *J. Struct. Eng.*, ASCE, **127**(1), 43-50.
- Hwang, S.J. and Lee, H.J. (2002), "Strength prediction for discontinuity regions by softened strut-and-tie model", accepted by *J. Struct. Eng.*, ASCE.
- Lu, W.Y., Lin, I.J., Hwang, S.J. and Lin, Y.H. (2002), "Shear strength of high-strength concrete dapped-end beams", submitted to *Magazine of Concrete Research*.
- Mattock, A.H. and Chan, T.C. (1979), "Design and behavior of dapped-end beams", *PCI J.*, **24**(6), 28-45.
- PCI Design Handbook, (1999), 4th edition, Prestressed Concrete Institute, Chicago, Illinois.
- Schäfer, K. (1996), "Strut-and-tie models for the design of structural concrete", Notes of Workshop, Department of Civil Engineering, National Cheng Kung University, Tainan, Taiwan.
- Vecchio, F.J. and Collins, M.P. (1993), "Compression response of cracked reinforced concrete", *J. Struct. Eng.*, ASCE, **119**(12), 3590-3610.
- Zhang, L.X.B. and Hsu, T.T.C. (1998), "Behavior and analysis of 100MPa concrete membrane elements", *J. Struct. Eng.*, ASCE, **124**(1), 24-34.

## Notation

- $a$  : shear span defined by the PCI Design Handbook, measured from the center of support to the center of the hanger bars
- : nominal shear span
- $a'$  : actual shear span, measured from the center of support to the interface between the nib and the full-depth beam
- $a_s$  : depth of the diagonal strut
- $A_f$  : area of primary tensile steel resisting moment
- $A_h$  : area of horizontal hoops
- $A_n$  : area of primary tensile steel resisting tensile force  $N_c$
- $A_s$  : area of main dapped-end reinforcement

$A_{th}$	: area of the horizontal tie
$A_v$	: area of the vertical hoops
$A_{vh}$	: area of the hanger bars
$A_{str}$	: effective area of the diagonal strut
$b$	: width of the nib
$b_s$	: width of the diagonal strut
$C$	: resultant compressive force at section due to flexure
$C_d$	: diagonal compression
$C_{d,n}$	: nominal diagonal compressive strength
$d$	: effective depth of the nib
	: assumed direction of principal compressive stress of concrete
	: direction of the diagonal concrete strut
$D$	: compression force in the diagonal strut (negative for compression)
$E_c$	: elastic modulus of the concrete
$E_s$	: elastic modulus of the steel
$f'_c$	: compressive strength of the standard concrete cylinder
$f_h$	: average tensile stress in the horizontal tie
$f_{yh}$	: yield stress of the horizontal hoop
$f_{yvh}$	: yield strength of the hanger bars
$F_h$	: tension force in the horizontal tie (positive for tension)
$\bar{F}_h$	: the balanced amount of the horizontal tie force
$F_{yh}$	: yielding force of the horizontal ties
$h$	: direction of the horizontal hoops
	: overall depth of the nib
$j, k$	: coefficients
$K$	: strut-and-tie index
$K_d$	: diagonal strut index
$K_h$	: the horizontal tie index
$\bar{K}_h$	: horizontal tie index with sufficient horizontal reinforcement
$jd$	: distance of the lever arm from the resultant compressive force to the centroid of the flexural tension reinforcement
$kd$	: depth of compression zone at the section
$M_n$	: nominal moment strength of the nib
$n$	: modular ratio of elasticity
	: $E_s/E_c$
$N_c$	: horizontal force due to restrained shrinkage, creep, or temperature change
$P_u$	: ultimate load measured in the test
$r$	: direction perpendicular to $d$
	: assumed direction of principal tensile stress
$R_d, R_h$	: ratios of the shear carried by the diagonal and horizontal mechanisms, respectively
$T$	: tension in the main dapped-end reinforcement
$v$	: direction of the vertical web reinforcement
$V_{dh}, V_{dv}$	: horizontal and vertical shear forces, respectively
$V_{dv, calc}$	: predicted shear strength of dapped-end beams
$V_{dv, test}$	: the shear strength of dapped-end beams measured in the test
$\gamma_h$	: fraction of horizontal shear transferred by the horizontal tie in the absence of the vertical tie
$\epsilon_o$	: concrete cylinder strain corresponding to the cylinder strength $f'_c$
	: $0.002 + 0.001 (f'_c - 20)/80$ ( $f'_c$ in units of MPa)
$\epsilon_d, \epsilon_r$	: average principal strains in the $d$ - and $r$ - directions, respectively (positive for tensile strain)
$\epsilon_h, \epsilon_v$	: average normal strains in the $h$ - and $v$ - directions, respectively (positive for tensile strain)
$\epsilon_{yh}$	: yield strain of the horizontal hoop
$\theta$	: angle of inclination of h-axis with respect to d-axis

$\rho$	: ratio of the main dapped-end reinforcement
$\rho_f$	: ratio of the flexural tensile reinforcement
$\rho_h$	: ratio of horizontal hoops
	: $A_h/bd$
$\zeta$	: softening coefficient of concrete in compression
$\sigma_d$	: average principal stress of concrete in the $d$ - directions (positive for tension)
$\sigma_{d, \max}$	: maximum compressive stress on the nodal zone (negative for compression)
$\mu$	: friction coefficient
$\lambda$	: coefficient for type of concrete